Available online at www.sciencedirect.com
SCIENCE DIRECT®
Journal of Nuclear Materials 351 (2006) 119–132
journal of nuclear materials
www.elsevier.com/locate/jnucmat

Helium–self-interstitial atom interaction in α-iron

Lisa Ventelon [a], Brian Wirth [a,*], Christophe Domain [b]

[a] Nuclear Engineering Department, UC Berkeley, Berkeley, CA 94720-1730, USA
[b] Electricité de France, EDF – R&D, Les Renardières, Departement MMC, 77250 Moret sur Loing, France

Abstract

The effect of He impurities on the properties and behavior of self-interstitial atom (SIA) clusters in α-Fe has been simulated by atomistic molecular dynamics (MD) and molecular statics (MS) simulation techniques using semi-empirical interatomic potentials and compared to ab initio electronic structure calculations. The MD simulations reveal many interactions between He and SIA clusters, including a spontaneous SIA–substitutional He recombination and replacement mechanism that ejects He into interstitial positions and a strong interaction between He, in either interstitial or substitutional positions, with SIA and SIA clusters and also with other He atoms. The MS calculations reveal relatively small interaction trapping radii of about 1 nm between interstitial He and SIA cluster complexes, but strong binding energies from 1.3 to 4.4 eV, depending on cluster size and interaction geometry. The comparisons between the ab initio and semi-empirical interactions are in generally good agreement and indicate that the He–point defect interactions in bcc Fe are well represented by considering the displacement (strain) field interactions amongst the defects.

1. Introduction

The large amount of helium generated from (n, α) reactions in first wall and blanket structures is a significant challenge associated with the development of long-lived and high-performance fusion materials [1]. Helium has a strong tendency to precipitate into thermally stable helium–vacancy clusters and helium bubbles within grain interiors, which can produce irradiation strengthening or assist the nucleation and growth of cavities, leading to swelling detrimental to the mechanical properties of metals and alloys. Moreover, helium migration to and precipitation into bubbles at the grain boundary is a cause of high temperature embrittlement [2–6]. Multiscale damage accumulation models currently under development for fusion materials require information about the migration behavior of He in interstitial or substitutional positions in the α-Fe lattice and the mobility and thermal stability of small vacancy–He clusters that serve as void or He bubble nuclei. As well, mechanistic insight into possible reactions, including the trapping and de-trapping of substitutional or interstitial He with numerous microstructural defects, including individual vacancies, self-interstitial atoms (SIA) and SIA clusters, dislocations, grain boundaries, and precipitate interfaces is required. The primary focus of this work is to enhance knowledge of the

* Corresponding author. Tel.: +1 510 642 5341; fax: +1 510 643 9685.
E-mail address: bdwirth@nuc.berkeley.edu (B. Wirth).

0022-3115/$ - see front matter © 2006 Elsevier B.V. All rights reserved.
doi:10.1016/j.jnucmat.2006.02.029

interactions between SIA and SIA clusters with interstitial and substitutional helium in α-iron.

It is known that self-interstitial atoms in metals interact with substitutional He, resulting in SIA–vacancy recombination and replacement of the He to an interstitial position in the metallic lattice [7,8]. However, the correspondence between the binding energies and interaction radii obtained from the pair potential-based interatomic interactions used in molecular dynamics simulations performed in the 1970s and 1980s [9,10] compared to the more recent *N*-body Finnis–Sinclair potentials is not known. As well, the interactions between SIA and SIA clusters with interstitial He has not been previously studied with atomistic simulations. Thus the effect of interstitial He on the properties and behavior of self-interstitial atom clusters in α-Fe has been calculated using atomistic molecular dynamics (MD) simulations to address the possible interactions and compared to ab initio electronic structure calculations to determine whether they can be understood based on classical concepts of elastic strain resulting from different atomic sizes (He and SIA) and displacement fields, or whether complex chemical and electronic structure effects govern the observed behavior.

2. Methodology

Atomistic simulations have been performed with semi-empirical Fe–He potentials, using both molecular dynamics (MD) and molecular statics (MS) using conjugate gradients. The Fe–Fe interaction is described by the Ackland version of the Finnis–Sinclair potential [11], which predicts a ⟨1 1 0⟩ dumbbell as the stable self-interstitial atom, with a metastable ⟨1 1 1⟩ dumbbell. According to this potential, the isolated SIA migrates by rotation of the ⟨1 1 0⟩ mono-interstitial to the ⟨1 1 1⟩-configuration with an activation energy of about 0.2 eV, followed by a fast migration in the ⟨1 1 1⟩ direction [12–14]. It is important to note that recent ab initio calculations [15–17], in addition to a new semi-empirical potential for Fe [18], predict a larger energy difference of 0.7 eV between the ⟨1 1 0⟩ and the ⟨1 1 1⟩ SIA configurations and migration by a different mechanism involving the translation and rotation of the ⟨1 1 0⟩ dumbbell between neighboring lattice sites. Yet, the activation energy for SIA migration is comparable, at about 0.3 eV, to that obtained with the earlier Ackland [11], Johnson [19] and Finnis and Sinclair [12,20] potentials and much lower than the value for vacancy migration. For larger SIA clusters, both sets of Fe potentials predict a ⟨1 1 1⟩ orientation of individual dumbbells within the cluster. Therefore, these potentials are comparable in terms of qualitative SIA and SIA cluster behavior, and the use of the new Fe potential will likely only result in small changes in the quantitative, but not qualitative results.

The Fe–He and He–He interactions are described by pair-wise potentials. The Fe–He interaction was recently fit by Morishita [5] to Hartree–Fock–Slater (HFS) calculations using the modified Wedepohl method performed by Wilson in the 1980s [19]. This potential is essentially purely repulsive. The Beck [21] potential is used to describe the He–He interactions.

Ab initio calculations have been performed with the Vienna Ab initio Simulation Package (VASP) [22–24]. The calculations implement a plane-wave basis set, using ultra-soft pseudo-potentials within the projector augmented wave (PAW) formalism to describe the electron-ion interaction [25,26]. Electron exchange and correlation are described by the Perdew–Zunger functional, adding a non-local correction in the form of the generalised gradient approximation (GGA) of Perdew and Wang. All the calculations were performed with the spin polarised GGA pseudo-potentials from the VASP library. Brillouin zone (BZ) sampling is performed using the Monkhorst–Pack scheme. Point defects as well as pure phases are investigated using the super-cell approach with periodic boundary conditions. The defect calculations are performed at constant volume, thus relaxing only the atomic position by conjugate gradient in a super-cell dimensioned with the equilibrium lattice parameter for Fe. Constant volume calculations lead to a slight overestimation of formation energies and underestimation of interaction energies, whereas volume relaxation calculations may lead to opposite effects. Nevertheless, the error for interstitial type defects, for which the relaxation volume is the largest, can be expected to be a few tenth of eV for 54 atom super-cells and up to 0.1 eV for 128 atom super-cells cells and usually the stability order of different configurations is not changed [17,27]. Calculations with 54 (or 128) atom super-cells are done with a BZ sampling of 125 (or 27) *k* points and a cut-off energy of 400 eV.

The semi-empirical MD simulations have been performed using a computational cell of $50a_0 \times 50a_0 \times 50a_0$ (containing 250 000 atoms) or $100a_0 \times 100a_0 \times 100a_0$ (containing 2 000 000 atoms) unit

cells, where a_0 is the Fe lattice parameter and periodic boundary conditions have been applied in all directions. In the conjugate gradient simulations, which use the same interatomic potentials, a cell size of $50a_0 \times 50a_0 \times 50a_0$ (containing 250 000 atoms) has been used, in addition to a study that systematically varied the cell size from $3a_0 \times 3a_0 \times 3a_0$ to $20a_0 \times 20a_0 \times 20a_0$. The conjugate gradient simulations have been used to investigate defect–defect formation and binding energies with full relaxation of the atomic positions around the defect(s) and volume relaxation. Notably, volume relaxation had only a minimal effect on the binding and formation energies.

The molecular statics calculations, performed either with the semi-empirical potentials or using the ultra-soft pseudo-potentials in the first principles method, provide the binding energy between two defect entities, A and B, in a bcc iron matrix containing N atoms, as follows. The energy, $E(N-1+A)$, of a super-cell containing only defect A is added to the corresponding energy, $E(N-1+B)$, of the super-cell containing only defect B. From this sum, the energy, $E(N-2+A+B)$, of the same super-cell containing both A and B defects is subtracted, as is the reference state (E_{ref}) of the super-cell containing no defect. Thus:

$$E_{\mathrm{b}}(AB) = [E(N-1+A) + E(N-1+B)] - [E(N-2+A+B) + E_{\mathrm{ref}}]. \quad (1)$$

This method can be easily extended to three, four and so on entities, to calculate the total binding energy as

$$E_{\mathrm{b}}(A_1A_2\ldots A_n) = \sum_{i=1}^{n} E(A_i) - [E(A_1 + A_2 + \cdots + A_n) + (n-1)E_{\mathrm{ref}}]. \quad (2)$$

For substitutional He, the reference state is the fcc crystal structure. Details of the calculation methods of the formation and binding energies are described in Ref. [28] for molecular statics simulations using semi-empirical potentials, and in Ref. [29] for ab initio calculations.

3. Results and discussion

It is well established that helium produced by (n,α) reactions initially resides in interstitial positions in metallic alloys, producing a large local distortion to the neighboring metal atoms, and possessing a very high mobility [19,7,30]. As interstitial helium diffuses in a metal with high vacancy supersaturation, as during irradiation, it will jump into a vacant lattice site, becoming substitutional with a large binding energy (strongly trapped). Subsequent diffusion of the now substitutional He atom can occur by a vacancy mechanism or by an interstitial mechanism following thermal dissociation (de-trapping) of He from the vacant lattice site or the replacement–recombination (kick-out) mechanism as a self-interstitial atom recombines with the vacant lattice site [4,7,8,19,30].

The semi-empirical potentials used in this work reveal that interstitial He diffuses from octahedral to neighboring octahedral interstitial sites through the tetrahedral saddle point with an activation energy of about 0.1 eV, in agreement with earlier studies [4,5,19,31]. Atomistic simulations of substitutional helium diffusion by a vacancy mechanism, performed within the framework of the multiple frequency diffusion model of Le Claire [32], reveal an effective activation energy of 2.35 eV for thermal helium diffusion and also show that substitutional helium can exchange with a second nearest neighbor vacancy with an activation energy of 0.66 eV [33]. Recent ab initio results show a reversal of the octahedral-tetrahedral site stability for interstitial He [34,35], but do reveal similar high mobility (low migrational activation energy) as an interstitial [35] and strong binding of energy of substitutional He to the vacant lattice site in which it resides [34,35].

The effect of He impurities on the properties and behavior of self-interstitial atom clusters in α-Fe has been investigated in this work by both molecular dynamics and molecular statics simulations, and the results are compared to ab initio calculations. Fig. 1 shows a comparison of the diffusivity of a 20 SIA cluster in pure iron and in the presence of 2500 atomic parts per million (ppm) of randomly distributed substitutional He atoms. The SIA cluster diffusivity was obtained from MD simulations in a $100a_0 \times 100a_0 \times 100a_0$ box at 600, 800 and 1000 K. As seen in Fig. 1, the presence of He has almost no effect on the temperature dependence of the SIA cluster diffusivity. The activation energy was below 0.1 eV in both pure Fe and Fe containing 2500 ppm substitutional He, increasing slightly from 0.06 to 0.08 eV with the addition of He. This indicates that the fundamental migration mechanism for the 20 SIA cluster remains the same and that the diffusion process is nearly athermal. However, the diffusion pre-factor does decrease by one

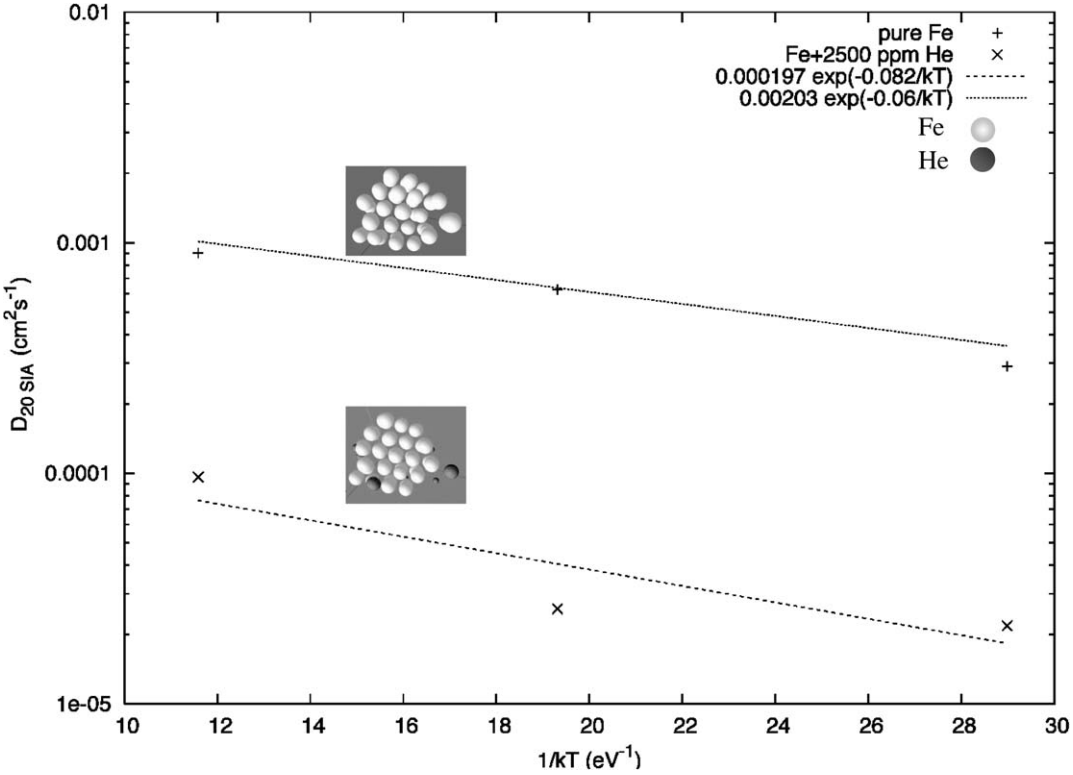

Fig. 1. Comparison of the diffusivities of a 20 SIA cluster obtained from MD simulations at 600, 800 and 1000 K in pure iron and in the presence of 2500 ppm of randomly distributed substitutional He atoms.

order of magnitude from 0.002 to 0.0002 cm^2/s with the addition of substitutional He, and indicates that He slows the net SIA cluster migration. Visualization of the MD simulations indicate that the effect of substitutional He on the migration of the 20 SIA cluster depends on the relative positions of both the He atoms and the SIA cluster.

Fig. 2 presents the results of an MD simulation performed in a $100a_0 \times 100a_0 \times 100a_0$ box at 1000 K in a defected region of otherwise perfect bcc iron containing 2500 ppm substitutional He. This simulation reveals a large number of interactions between He and point defect clusters. As shown in Fig. 2, a 9 SIA–He_1^i–He_1^s cluster, a single vacancy, an isolated SIA, an interstitial He atom and two substitutional He atoms are in close proximity within several nanometers (Fig. 2(a)). The isolated SIA is 2.3 nm away from the nearest of the two substitutional He atoms. Over several tens of picoseconds, the SIA migrates three-dimensionally with multiple changes of orientation, generally moving towards this helium atom. Upon reaching a separation distance of about 1.4 nm from the substitutional helium atom in the [1 1 1] direction (Fig. 2(b)), a fast and spontaneous recombination–replacement reaction occurs. In this reaction, the SIA enters the vacant lattice site, recombining with the vacancy and ejecting the helium atom from a substitutional to an interstitial position. The resulting interstitial He atom rapidly diffuses to and binds with the nearby substitutional He atom as a He_2V_1 complex (Fig. 2(c)), which is trapped and immobile for about 10 ps before dissociating (de-trapping). The 9 SIA–He_1^i–He_1^s cluster remains effectively trapped for the first 40 ps of the simulation (Fig. 2(a)–(c)), before de-trapping from the two (interstitial and substitutional) He atoms and migrating one-dimensionally towards the isolated vacancy (Fig. 2(c) and (d)), which it annihilates to become an 8 SIA cluster (Fig. 2(d)). Subsequently, the interstitial He atom migrates to and traps the 8 SIA cluster (Fig. 2(e)). Thus, the resulting defect structure observed after 60 ps at 1000 K consists of a trapped 8 SIA–1 He cluster, a di-He cluster (He_1^i–He_1^s), a substitutional He atom and a freely migrating interstitial He atom. This simulation reveals many interactions that merit further study to determine the interaction radii and trapping

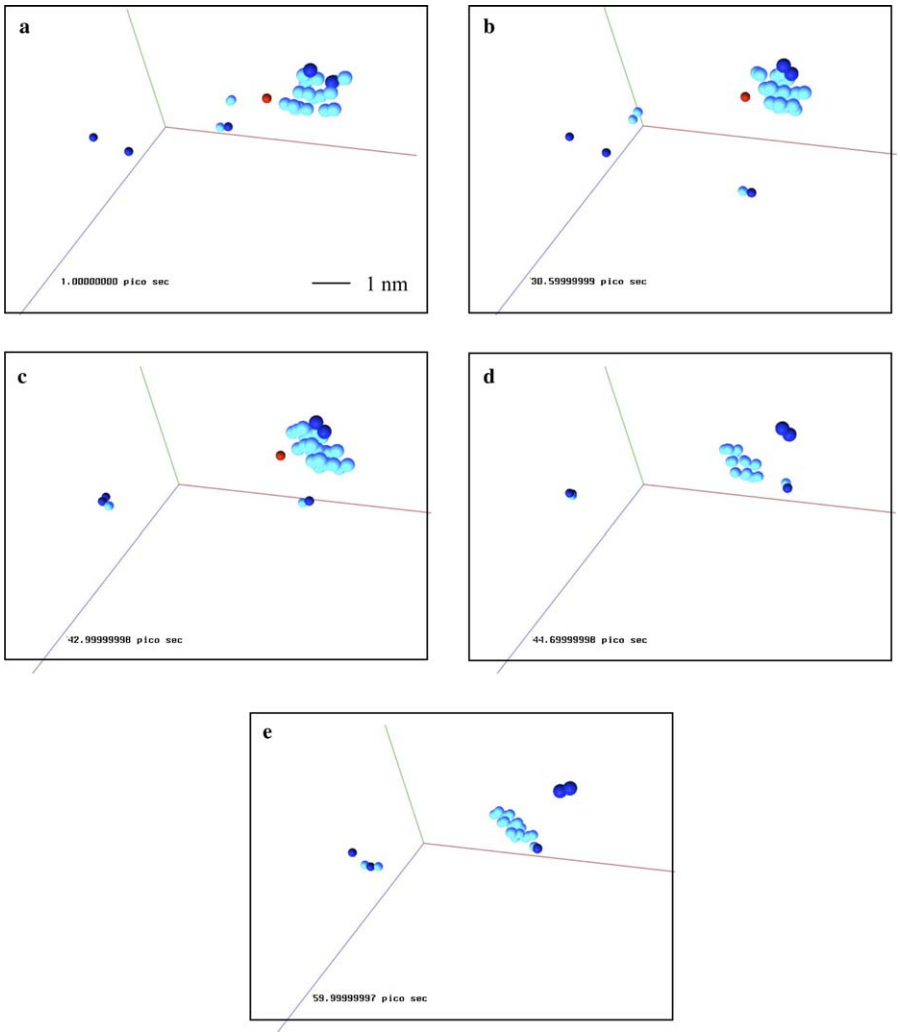

Fig. 2. Series of MD snapshots showing the interaction between a 9 SIA–He_1^i–He_1^s cluster, a neighboring vacancy, an isolated SIA, an interstitial He atom and two substitutional He atoms at 1000 K: (a) $t = 1$ ps. The SIAs are represented by light blue spheres, the He atoms by dark blue spheres, and the vacancies by red spheres. This simulation shows a spontaneous recombination–replacement reaction between the single SIA and a nearby substitutional He that ejects the He from a substitutional to an interstitial position: (b) $t = 30.6$ ps; interstitial He–substitutional He complex formation: (c) $t = 43$ ps; the de-trapping of a 9 SIA cluster from the di-He: (d) $t = 44.6$ ps; and migration of the interstitial He atom to the 8 SIA cluster: (e) $t = 60$ ps.

energies, including the SIA–substitutional helium recombination and replacement interaction, the He_1^i–He_1^i trapping interaction, and the trapping and de-trapping processes involving He and SIA clusters.

Fig. 3 shows a series of snapshots from an MD simulation of an 11 SIA cluster and a 4 substitutional He–2 vacancy cluster performed in a $100a_0 \times 100a_0 \times 100a_0$ box at 1000 K. The 11 SIA cluster, initially about 8 nm away from the He cluster in the [1 1 1] direction, migrates in a one-dimensional random walk along the [1 1 1] direction for about 20 ps (Fig. 3(a)). However, when the SIA cluster reaches a separation distance of about 2 nm from the He–vacancy cluster, the SIA cluster is spontaneously attracted to the vacancy cluster complex, where it annihilates (recombines with) the six vacant lattice sites, resulting in the ejection of the four substitutional He atoms into interstitial positions (Fig. 3(b)). The SIA cluster and 4 He interstitial atoms rapidly coalesce to form a 5 SIA–4 interstitial He cluster (Fig. 3(c)). Notably, the 5 SIA–4 interstitial He cluster does rotate from its initial [1 1 1] direction to the $[1\,\bar{1}\,1]$ direction (Fig. 3(d)). But, the resulting SIA–He cluster is strongly bound and, although the SIA cluster

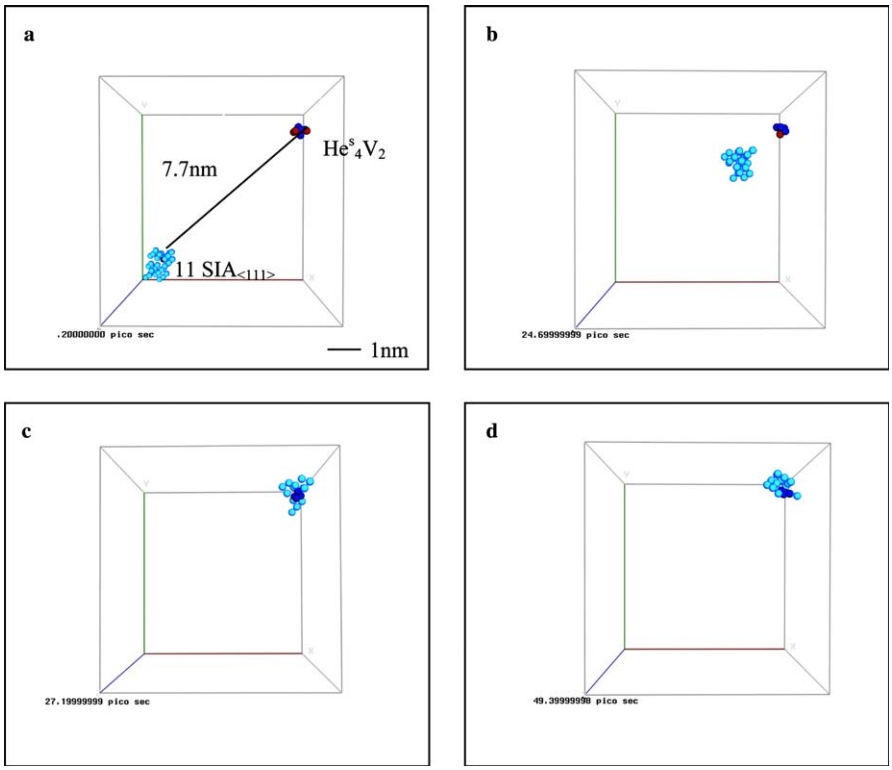

Fig. 3. Series of snapshots of the interaction between an 11 SIA cluster (light blue spheres) and 4 substitutional He (dark blue spheres)–2 vacancy cluster (red spheres) from an MD simulation at 1000 K: (a) $t = 0.2$ ps. The SIA cluster is spontaneously attracted to the vacancy cluster complex: (b) $t = 24.7$ ps; and annihilates the six vacancies, resulting in the ejection of the He atoms into interstitial positions: (c) $t = 27.2$ ps. The resulting 5 SIA–4 interstitial He cluster rotates from its initial $[1\,1\,1]$ direction to the direction $[1\,\bar{1}\,1]$, but is strongly bound: (d) $t = 49.4$ ps.

continually attempts to detach from the cluster and resume one-dimensional migration, it is unable to overcome the binding interaction and remains trapped over the resulting 100 ps of MD simulation.

Fig. 4 shows a series of snapshots from the MD simulation of a 20 SIA cluster and two interstitial helium atoms in a $50a_0 \times 50a_0 \times 50a_0$ box at 800 K. Initially, the nearest helium atom is about 2 nm from the SIA cluster and freely migrates three-dimensionally (Fig. 5(a)). After 13 ps, this helium atom migrates towards the SIA cluster and upon reaching a separation distance of about 0.7 nm (Fig. 5(b)), it is spontaneously attracted to the cluster and becomes trapped (Fig. 5(c)). The second interstitial helium atom moves randomly for 50 ps until reaching a distance of 0.8 nm from the 20 SIA–1 He cluster complex (Fig. 5(d)). It then also migrates rapidly to the cluster, forming the resulting 20 SIA–2 He cluster complex, which stays immobile over the next 100 ps of the simulation (Fig. 5(e)).

To summarize the molecular dynamics simulations presented in Figs. 1–4, a strong interaction between one-dimensionally gliding SIA clusters and substitutional He, as well as small He–vacancy clusters is observed, with spontaneous interaction radii of about 1.5 ± 0.5 nm, leading to vacancy–SIA recombination and a replacement (kick-out) mechanism that ejects substitutional He atoms into interstitial positions. The MD simulations also reveal that SIA cluster–interstitial He complexes can be moderately to strongly trapped, depending on the relative size of each cluster. However, these simulations do not provide a quantitative assessment of the recombination–replacement radii or the trapping–binding energetics. Therefore, we performed molecular statics (MS) calculations using the conjugate gradient method to investigate the energetics of interstitial He–SIA cluster complexes and compared the results of selected configurations to ab initio calculations. The specific geometry of the He–SIA cluster interactions investigated has

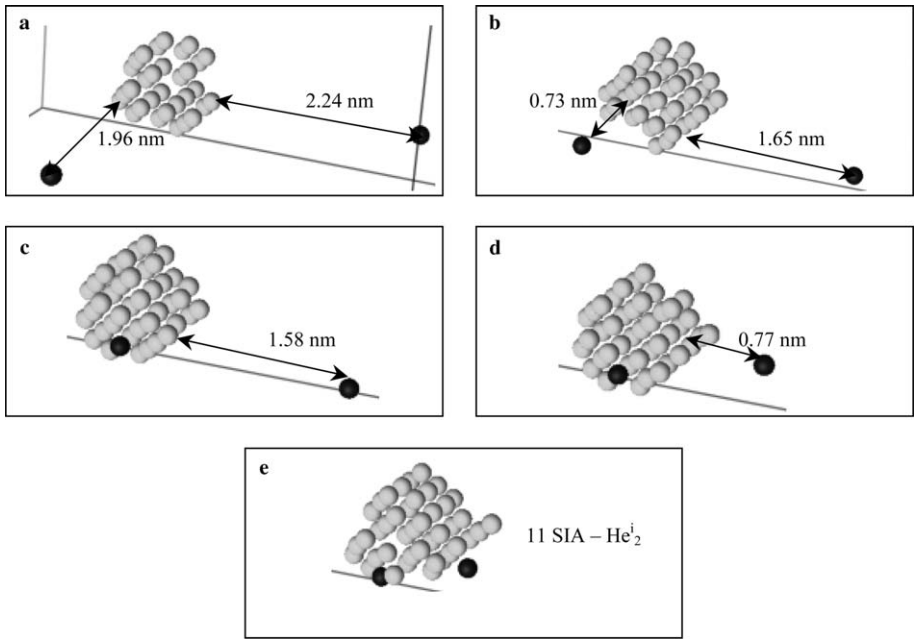

Fig. 4. Series of snapshots from a MD simulation at 800 K showing the interaction between a 20 SIA cluster (light grey spheres) and two interstitial He atoms (dark grey spheres), initially about 2 nm from the SIA cluster. After 13 ps, the helium on the lower left migrates towards the SIA cluster and upon reaching a separation of 0.7 nm (b), it spontaneously migrates to the SIA cluster and becomes strongly trapped (c). The second interstitial helium atom moves randomly for 50 ps until reaching a distance of about 0.8 nm from the 20 SIA–1 He cluster complex (d). It then migrates rapidly to the cluster, forming a 20 SIA–2 He complex which stays immobile over times of the order of 100 ps (e).

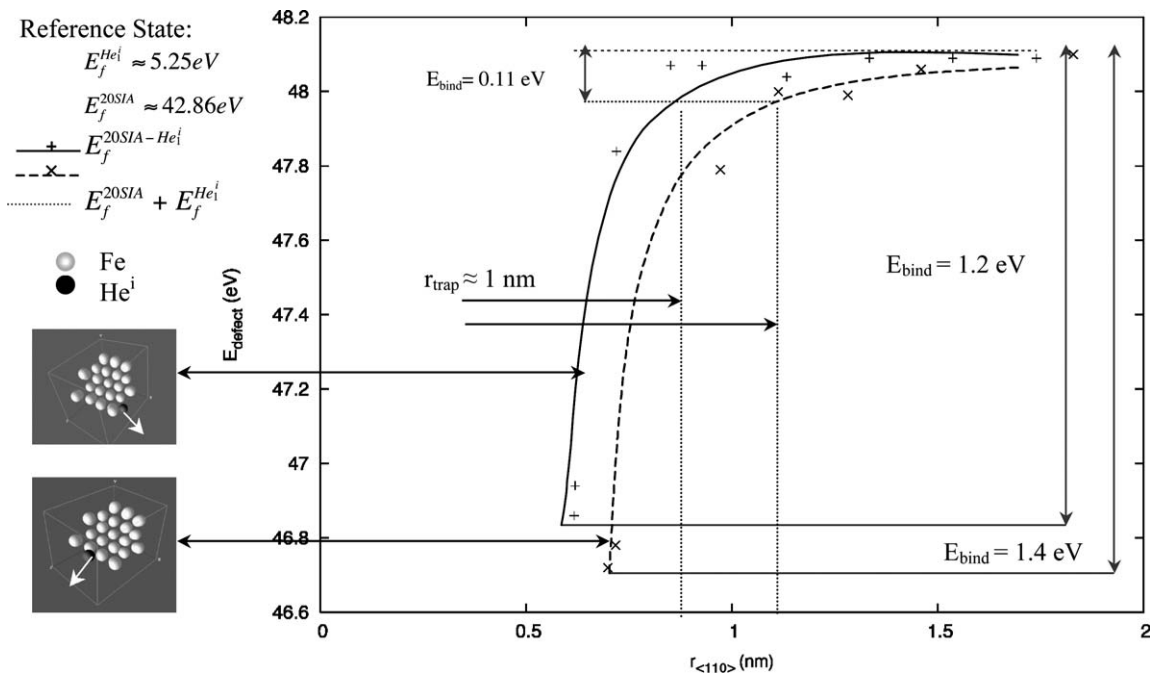

Fig. 5. Calculated defect energy of a 20 SIA–He$^i_1$ cluster from conjugate gradient MS calculations as a function of the distance between the center of mass of the SIA cluster and the He atom. Interstitial He has been displaced along a $\langle 1\,1\,0\rangle$ direction, perpendicular to the dumbbell orientation. The position of the jog point on the 20 SIA cluster is denoted by an arrow on the lower left inset diagram.

been selected from representative MD simulation results, as well as by considering the strain field interactions between the defects. For example, split interstitial dumbbells, whether isolated or as part of a small SIA cluster/dislocation loop, have a large anisotropic stress field, which is compressive along the orientation direction and tensile along the perpendicular direction. The displacement field of interstitial He is roughly spherical and compressive. Thus, the anticipated strain field interaction between these defects is expected to produce an attractive interaction along the direction perpendicular to the dumbbell(s) orientation and a repulsive interaction along its orientation.

Therefore, to provide a quantitative assessment of the binding energy between SIA clusters and interstitial He atom clusters, interstitial He has been displaced along a $\langle 1\,1\,0\rangle$ direction perpendicular to the $\langle 1\,1\,1\rangle$-orientation of the dumbbells within an SIA cluster. Fig. 5 shows the calculated defect energy of a 20 SIA–He_1^i cluster as a function of the distance between the center of mass of the SIA cluster and of the interstitial He atom. The pair has a formation energy of 48.1 eV when separated by more than 2 nm. As the He atom is moved towards the loop in the conjugate gradient calculations, a slightly positive binding energy of a few hundredths of an eV is obtained at a distance of about 1.5 nm. With further movement of the He atom towards the SIA cluster/loop periphery, a sharp decrease in the total defect energy (increase in binding energy) is observed. The maximum binding energy between the 20 SIA cluster/loop and the interstitial helium atom exists when the helium atom is positioned immediately next to the loop periphery (distance from center of cluster of approximately 0.5 nm) and is 1.2 eV when the He atom is on a perfect ledge, and increases to 1.4 eV when the He atom is close to a jog point (see the illustration of the configuration, inset in Fig. 5, for definition of the jog point). Presumably, the increase in binding energy is due to the higher strain energy associated with the 20 SIA cluster at the jog point. As expected, further movement of the He atom into the loop interior results in highly negative (repulsive) binding energies.

The trapping radius has been estimated by considering the interstitial He atom to be spontaneously attracted to the SIA cluster/loop when the binding energy exceeds the mean kinetic energy of the He atom. The internal energy of a monoatomic ideal gas atom, $E_k = 3/2kT$, has been used to estimate the mean kinetic energy. For He, this corresponds to a value of 0.1 ± 0.02 eV over the temperature range of 400–700 °C. The trapping (or interaction) radii obtained from this analysis range from 0.7 to 1.2 nm, depending on the specific orientation of the interaction between the interstitial helium and the 20-member SIA cluster loop. These values are in good agreement with the estimated spontaneous trapping radii of 0.7 and 0.8 nm for the trapping of interstitial He by a 20 SIA cluster at 800 K obtained from the MD results presented in Fig. 4.

The relatively strong binding energies of 1.2–1.4 eV of the trapped He_1^i–20 SIA complex are large enough to influence microstructural evolution. Assuming that the de-trapping rate of a bound cluster is given by a standard Arrhenius form, $k = v_0\exp(-(E_b + E_m)/kT)$ where k is the de-trapping rate, E_b is the binding energy, E_m is the migration energy of the (most) mobile species (assumed to be about 0.1 eV for both interstitial He and SIA clusters, based on MD simulations [32]), and v_0 is the intrinsic vibrational attempt frequency (assumed to be $\sim 10^{13}$ s^{-1}). The observed binding energies correspond to mean lifetimes ($=1/k$) for the trapped complex on the order of 100 ps to 1 μs at 700 °C and 500 °C, respectively.

Fig. 6 shows the results of conjugate gradient calculations performed for 20 SIA–He_2^i and 20 SIA–He_4^i configurations. As expected for the situation where cluster binding results from the overlap and canceling of tensile and compressive strain energy, the binding energies increase with increasing size of the helium interstitial clusters and depend on the specific geometry of the interaction (e.g., again the binding energies are strongest at the loop jog point). The trapping radii are increased slightly for the He_2^i and He_4^i compared to the single interstitial helium, but are rather small, on the order of 1.3–1.5 nm. The binding energies of 1.8 and 3.5 eV correspond to calculated mean trapping lifetimes on the order of 10 μs and one year at 500 °C for the 2 and the 4 He–20 SIA cluster complexes, respectively.

Fig. 7 plots the conjugate gradient results obtained for complexes containing 1, 2, and 4 interstitial helium with 1, 2, 6, 11, and 20 SIA clusters. Although there is a large amount of scatter in the data, the general trend is of increasing binding energy with increasing SIA and He cluster size. The data scatter is most likely due to the limited number of geometric configurations investigated and the specific details of those configurations (e.g. the relative position of the He atoms compared

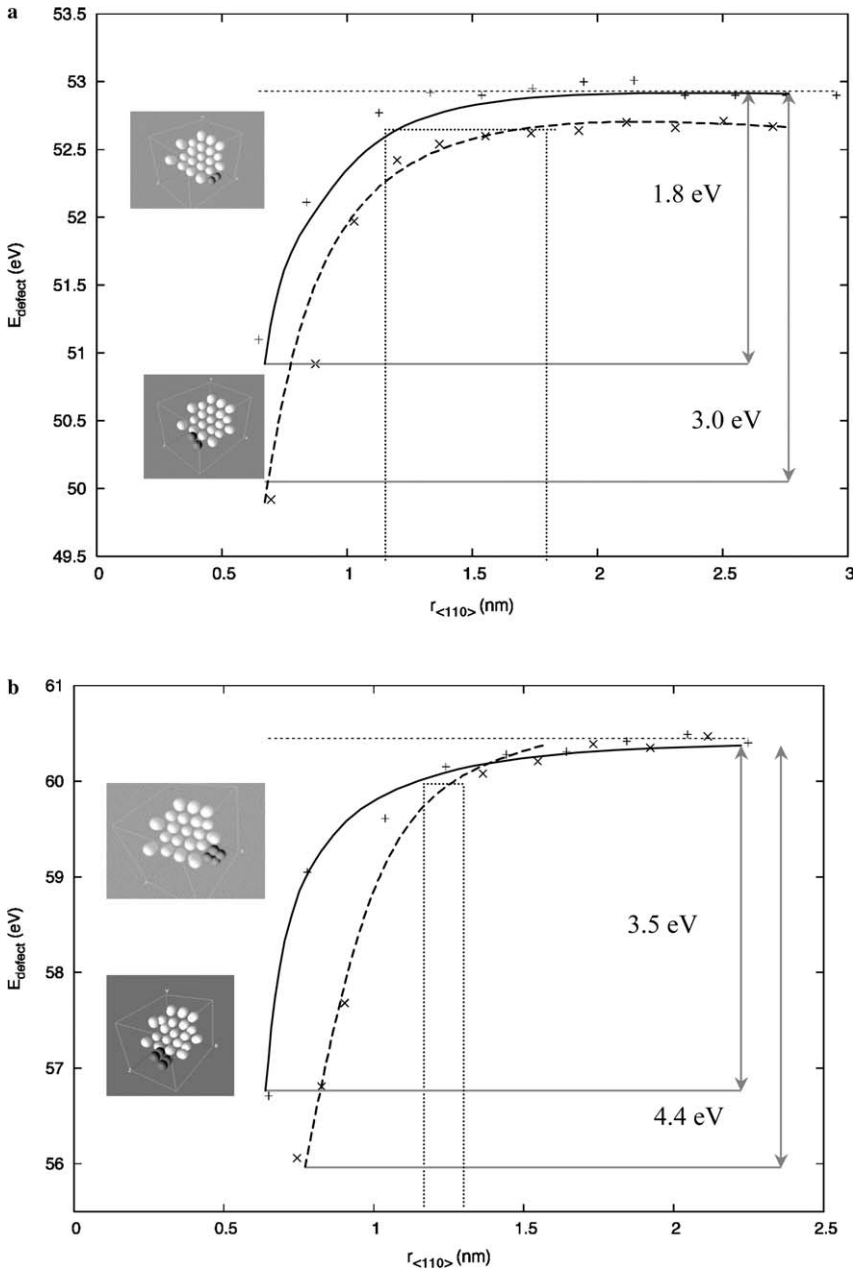

Fig. 6. Calculated defect energy for 20 SIA–He_2^i (a) and 20 SIA–He_4^i configurations (b) obtained from MS calculations.

to the cluster loop). We conclude that moderate to strong binding interactions ($E^b \sim 1$–4 eV) and trapping will occur between interstitial He and either a single SIA or SIA clusters containing between 2 and 20 SIAs. Notably, the trapping radii governing the interaction are rather small, on the order of 1 nm. The small trapping radii are consistent with, and actually slightly larger than the values of 0.3–0.7 nm obtained by Kurtz and Heinisch for interstitial He interaction with grain boundaries in Fe [36].

A key question to ask is about the adequacy of the semi-empirical potentials used in this work. Thus, we have compared the interaction energies obtained from our semi-empirical MS simulations to ab initio electronic structure calculations. Table 1 provides a comparison of (i) the formation energy of substitutional and interstitial helium, (ii) the

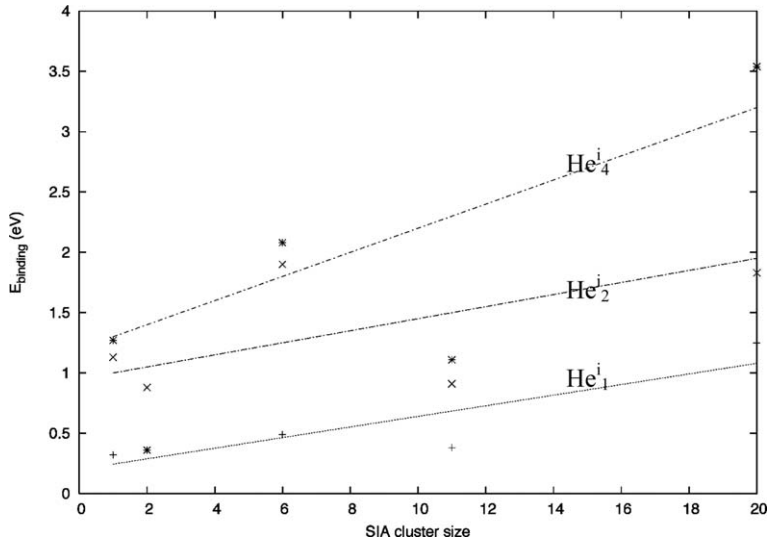

Fig. 7. The binding energies of complexes containing 1, 2, and 4 interstitial helium with 1, 2, 6, 11, and 20 SIA clusters obtained from conjugate gradient molecular statics calculations.

Table 1
Comparison of the interaction energies obtained from the semi-empirical MS simulations to ab initio electronic structure calculations, formation energy of a substitutional and an interstitial He atom, binding energy between two interstitial He atoms, one interstitial and one substitutional He atom, and one substitutional and a vacancy

Configuration	Ab initio results (54 atoms)	Semi-empirical results (250 000 atoms)
He occupation site (eV)		
He^s_1	$E_f = 4.3$	$E_f = 3.25$
He^i_1	$E_f = 4.6$	$E_f = 5.75$ $E_m = 0.1$
	He^i tetrahedral	He^i octahedral
		Tetrahedral saddle
He^i_1–He^i_1 binding energy (eV)		
cfg1	0.3	0.4
cfg2	0.4	0.8
He^i–He^s binding energy (eV)		
He^i_1–He^s_1 ⟨100⟩	1.8	2.2
⟨110⟩	1.9	2.1
He^i_2–He^s_1	3.6	4.3
He^i_3–He^s_1	5.0	5.5
He^i_4–He^s_1	6.6	8.1
He^i_5–He^s_1	8.4	9.7
He^s_1–vacancy binding energy (eV)		
1 nn	0.8	0.3
2 nn	0.5	0.2

Corresponding configurations are presented in Figs. 8 and 9.

binding energy between helium interstitial atoms, (iii) the binding energy between a substitutional He atom with 1–5 helium atoms, and (iv) the binding energy between substitutional helium and an additional vacancy in the bcc iron lattice. In this comparison, the ab initio calculations have been performed using the VASP code in a 54 atom computational cell, consisting of $3a_0 \times 3a_0 \times 3a_0$ bcc unit cells, plus the indicated number of helium atoms. The semi-empirical calculations have been performed using conjugate gradient relaxation in a 250 000 atom computational cell, consisting of $50a_0 \times 50a_0 \times 50a_0$ bcc unit cells, plus the indicated number of helium atoms.

The calculated formation energy of substitutional He is 1 eV larger in the ab initio calculations than is obtained with the semi-empirical potentials, while that of the interstitial He atom is about 0.6 eV smaller. As previously mentioned, there is also a difference in the stable position of the helium interstitial atom in the bcc Fe lattice, with the ab initio calculations predicting a tetrahedral rather than an octahedral position. Because of the site reversal for interstitial He, the semi-empirical molecular statics calculations presented in the comparison below have been performed with the same arrangement of multiple He atoms, albeit with the He shifted into equivalent position(s) on the octahedral, rather than the tetrahedral sub-lattice (see Fig. 8).

Both approaches predict the same lowest energy configuration for the di-interstitial He (He^i_1–He^i_1) cluster, although the semi-empirical potential results give slightly higher binding energies by 0.1–0.4 eV. These positive binding energies indicate the possibility of forming bound di-interstitial He clusters, and

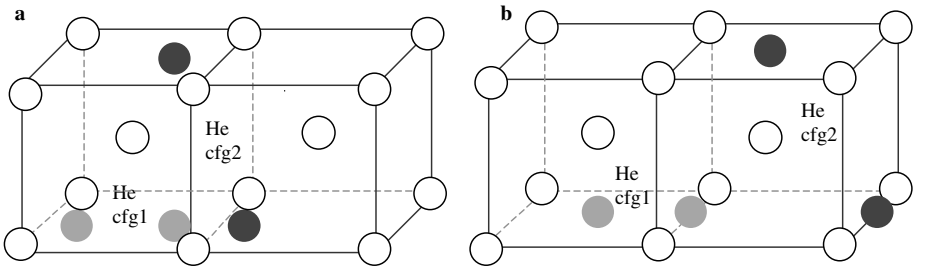

Fig. 8. Interstitial helium pair for the $\langle 0\,1\,0\rangle$ (cfg1) and the $\langle 0\,\bar{1}\,2\rangle$ (cfg2) orientations. The He interstitial atoms sit on tetrahedral sites in the VASP calculation (a), while the positions are shifted to octahedral sites for the semi-empirical MS calculation (b). Ab initio and semi-empirical calculation results corresponding to these two configurations are presented in Table 1.

more strongly bound He_1^i–He_1^s clusters. Indeed, a He_1^i–He_1^s cluster was observed in the MD simulations following the detachment of a 9 SIA cluster, as shown in Fig. 2, and the observed cluster stability is consistent with the binding energies presented in Table 1. We have also compared the binding energies between a substitutional He atom with one to five neighboring interstitial He atoms. Again, the interstitial He atoms are inserted on tetrahedral sites in the VASP and octahedral sites in the MS calculations. As listed in Table 1, both approaches show an increasing binding energy with increasing number of interstitial He atoms within the cluster, from about 2 eV to 9.7 eV. A comparison between the two approaches reveals that the binding energies are higher for the semi-empirical potential relative to the ab initio calculations by 0.2–1.5 eV, with the configurations with the larger number of He atoms having the largest discrepancy. The qualitative trends are in good agreement, although a different lowest energy configuration is obtained for the helium substitutional–helium interstitial cluster. In this case, the ab initio calculations predict a 'split-dumbbell' configuration of two helium atoms sharing one bcc lattice site, with lowest energy associated with a $\langle 1\,1\,0\rangle$ orientation of the dumbbell, whereas the semi-empirical calculations indicate that the $\langle 1\,0\,0\rangle$ orientation is energetically favored. However, both calculations indicate that the difference in energy between the two configurations is small and less than 0.1 eV.

The energy and configurations of a substitutional He atom with a nearest neighbor vacancy (at either first or second nearest neighbor, 1 nn and 2 nn, positions) has also been compared. Both methods predict that the He_1^s–nearest neighbor vacancy complex is energetically preferred. As well, both methods predict that the He atom is not situated on a perfect lattice site, but rather in an interstitial position between the two lattice sites. The ab initio results predict larger binding energies for the substitutional helium–vacancy complex by 0.3–0.5 eV compared to the semi-empirical potential, whereas smaller binding energies were predicted for the multiple helium atom clusters. In addition, the ab initio results predict that the He atom relaxes symmetrically between the initial substitutional site and the additional vacant site for both first and second nearest neighbor positions, while the semi-empirical results predict a non-symmetric configuration of the He atom (Fig. 9).

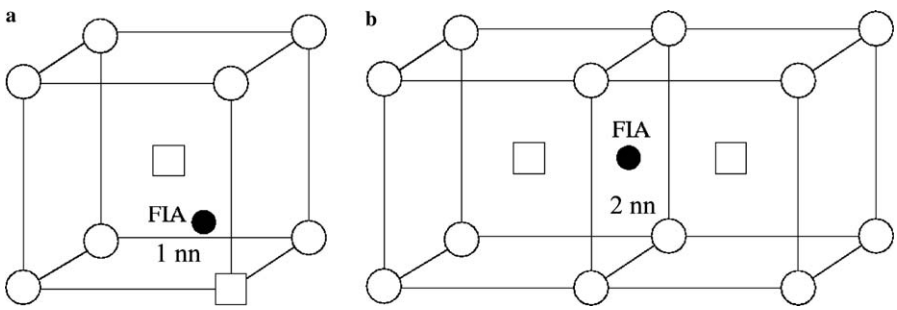

Fig. 9. Relaxed configurations from ab initio calculations of a foreign He interstitial atom (FIA), represented by a black sphere, binding to a nearest neighbor vacancy (white square) at either first nearest neighbor, 1 nn (a) or second nearest neighbor, 2 nn (b). Corresponding calculation results are presented in Table 1.

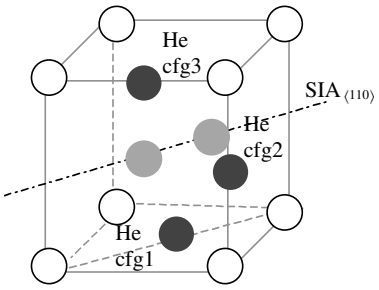

Fig. 10. Three different configurations (cfg1, cfg2, cfg3) used to calculate the interstitial He atom (dark gray spheres)–self-interstitial atom (light gray spheres) binding energies presented in Table 2.

Three different configurations of interstitial helium with a ⟨1 1 0⟩-oriented self-interstitial atom, as shown in Fig. 10, were used as a final comparison. The ab initio calculations were performed with both 54 atom ($3a_0 \times 3a_0 \times 3a_0$) and 128 atom ($4a_0 \times 4a_0 \times 4a_0$) unit cells containing 1 self-interstitial atom and 1 interstitial He atom, while the semi-empirical MS calculations were performed by systematically varying the cell-size from $3a_0 \times 3a_0 \times 3a_0$ (54 atoms) to $20a_0 \times 20a_0 \times 20a_0$ (16000 atoms) containing 1 self-interstitial atom and 1 interstitial He atom. Table 2 presents the results obtained for computational cell sizes of 54 and 128 atoms. In these calculations, He has been introduced on octahedral sites in the ab initio calculation, even though the preferred configuration for (isolated) interstitial He is the tetrahedral site.

Table 2
Comparison of the binding energies (in eV) between a ⟨1 1 0⟩-oriented Fe SIA and a neighboring interstitial He atom (shown in Fig. 10) obtained from ab initio and semi-empirical calculations for two different cell sizes, 54 and 128 atoms

Configuration	Ab initio results		Semi-empirical results	
	54 atoms	128 atoms	54 atoms	128 atoms
He_1^i cfg1	−0.15	−0.09	0.32	0.34
He_1^i cfg2	−0.04	0.03	−0.15	−0.09
He_1^i cfg3	0.02	0.07	0.29	0.37

Both approaches predict that configuration 3 is energetically preferred, although the semi-empirical potentials predict a change in the relative stability between configuration 1 and 3 with increasing from 54 to 128 atom cell size. The difference in binding energies between the ab initio and semi-empirical calculations is between −0.12 and 0.47 eV, is nearly independent of the cell size and reasonably consistent with the results presented in Table 1. However, the relative stability of the three configurations predicted by the ab initio and semi-empirical approaches is not the same. In the ab initio calculations, configuration 1 has a repulsive interaction, while the semi-empirical potentials predict that configuration 2 is repulsive. Thus, while the quantitative agreement for the SIA–He_1^i binding energy between the methods is reasonably consistent with the other configurations

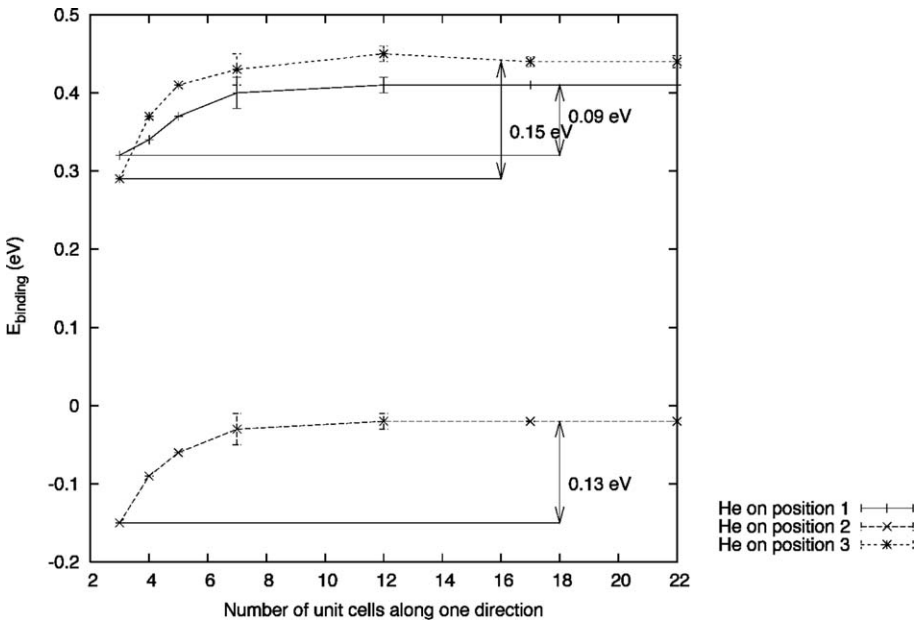

Fig. 11. SIA–He interstitial binding energy versus the number of unit cells for each of the three configurations presented in Fig. 10.

investigated, the comparison of the predicted relative stability is no longer as good. The reasons for the difference in the relative stability of the SIA–helium interstitial configurations are not fully understood.

One possibility relates to the comparison between calculations with small computational cells, where image and strain interactions associated with the use of periodic boundary conditions could be different for the three different configurations. As observed in the results presented in Table 1, the quantitative agreement between the ab initio and semi-empirical potentials became worse as the number of He interstitials, and correspondingly, the strain energy increased. Fig. 11 presents the results of a size scaling study on the SIA–He interstitial binding energy for each of the three configurations obtained from the semi-empirical potentials. The results indicate a strong cell-size effect on the resulting binding energy that does not diminish until larger system sizes on the order of $10a_0 \times 10a_0 \times 10a_0$. The difference in calculated binding energy for the configurations upon increasing the cell size from $3a_0 \times 3a_0 \times 3a_0$ unit cells to $20a_0 \times 20a_0 \times 20a_0$ was configuration dependent. The largest change in binding energy was 0.15 eV for configuration 3, while the smallest change of 0.09 eV was obtained for configuration 1. The increase in binding energy, averaged over all three configurations, with increasing the cell size and thereby decreasing the image strain energy within the computation, was equal to 0.12 ± 0.03 eV. This value is consistent with the under-estimate of interaction energies on the order of a few tenths of eV obtained in other ab initio studies with constant volume calculations [17,27]. The most striking result of the size scaling study presented in Fig. 11 is the reversal in the relative stability between configurations. This reinforces the knowledge that care must be taken in accounting for strain interactions from the use of periodic boundary conditions with small simulation cells, and indicates that additional ab initio calculations are required for a complete and quantitative validation of the semi-empirical potentials.

However, aside from the treatment of periodic image interactions and some subtle differences in the stable configuration of interstitial He and the He_1^i–He_1^s split-dumbbell, the ab initio and semi-empirical potential calculations results presented in Tables 1 and 2 are in reasonably good agreement. The overall consistency of the results provides confidence that the semi-empirical potentials do accurately represent helium–point defect interactions in Fe. The binding energies obtained from the semi-empirical potentials for helium–helium and helium–self-interstitial cluster complexes are larger than the ab initio values by 0.2–1.5 eV and may indicate that the helium–iron repulsive interaction in the pair potential is too stiff (repulsive) at short interatomic separations, or rather they may be indicative of periodic image effects. Notably, there is no indication from the results that complex electronic structure effects are dictating the observed behavior. Thus He–defect interactions in Fe are reliably predicted by the semi-empirical potentials used in this work, and perhaps more importantly, the interactions are well described by considering the elastic strain interactions, which provides a continuum mechanics basis for interpreting the complex dynamics observed between He and SIA cluster defects, and extrapolating these results.

4. Conclusions

The results of atomistic calculations to investigate the effect of He impurities on the properties and behavior of self-interstitial atom clusters in Fe have been presented, in addition to a comparison between ab initio and semi-empirical potential calculations. The MD simulations using semi-empirical potentials reveal a high mobility of interstitial He in bcc Fe, a spontaneous SIA–substitutional He recombination and replacement mechanism that ejects He into interstitial positions, and a strong interaction between He, in either interstitial or substitutional positions, with SIA and SIA clusters.

The MS calculations reveal relatively small interaction trapping radii of about 1 nm between interstitial He and SIA cluster complexes, but with strong binding energies from about 1.3 to 4.4 eV. The strong binding interactions can effectively trap the otherwise highly mobile SIA clusters for sufficiently long periods of time to influence the overall microstructural evolution under fusion neutron irradiation conditions. Overall, the results obtained from the semi-empirical potentials are in good qualitative agreement with ab initio results and indicate that bound helium–helium and helium–SIA cluster complexes can form and that the helium–SIA interactions are governed by elastic interactions between the He and SIA. Future work will focus on further validation of the semi-empirical potentials and investigating the migration mechanisms and mobility of substitutional helium–vacancy cluster complexes using kinetic Monte Carlo simulations.

Acknowledgements

The authors would like to acknowledge Professor G. Robert Odette (UCSB) and Drs Takuya Yamamoto (UCSB), Rick Kurtz, Howard Heinisch and Fei Gao (PNNL) and François Willaime and Chu Chun Fu (CEA/Saclay) for many helpful discussions during the course of this work. This work has been supported by the Office of Fusion Energy Sciences, US Department of Energy under Grant DE-FG02-04ER54750, and partly supported by the European PERFECT project (FI60-CT-2003-508840).

References

[1] E.E. Bloom, J. Nucl. Mater. 7 (1998) 258.
[2] H. Ullmaier, Rad. Effects 78 (1983) 1.
[3] S. Jitsukawa, A. Kinura, A. Kohyama, R.L. Kluch, A.A. Tavassoli, B. van der Schaaf, G.R. Odette, J.W. Rensman, M. Victoria, C. Petersen, J. Nucl. Mater. 329–333 (2004) 39.
[4] D.J. Reed, Rad. Effects 31 (1977) 129.
[5] K. Morishita, R. Sugano, B.D. Wirth, T. Diaz de la Rubia, Nucl. Instrum. and Meth. B 202 (2003) 76.
[6] L.K. Mansur, M.L. Grossbeck, J. Nucl. Mater. 155–157 (1988) 130.
[7] L.K. Mansur, E.H. Lee, P.J. Maziasz, A.P. Rowcliffe, J. Nucl. Mater. 141–143 (1986) 633.
[8] N.M. Ghoniem, S. Sharafat, J.M. Williams, L.K. Mansur, J. Nucl. Mater. 117 (1983) 96.
[9] W.D. Wilson, C.L. Bisson, Rad. Effects 22 (1974) 1.
[10] W.D. Wilson, C.L. Bisson, Rad. Effects 25 (1975) 197.
[11] G.J. Ackland, D.J. Bacon, A.F. Calder, T. Harry, Philos. Mag. A 75 (1997) 713.
[12] B.D. Wirth, G.R. Odette, D. Maroudas, G.E. Lucas, J. Nucl. Mater. 244 (1997) 185.
[13] N. Soneda, T. Diaz de la Rubia, Philos. Mag. A 78 (1998) 959.
[14] Y.N. Osetsky, D.J. Bacon, A. Serra, B.N. Singh, S.I.Y. Golubov, J. Nucl. Mater. 276 (2000) 65.
[15] C.C. Fu, F. Willaime, P. Ordejón, Phys. Rev. Lett. 92 (2004) 175503.
[16] F. Willaime, C.C. Fu, M.C. Marinica, J. Dalla Torre, Nucl. Instrum. and Meth. B 228 (2005) 92.
[17] C. Domain, C.S. Becquart, Phys. Rev. B 65 (2002) 024103.
[18] M.I. Mendelev, S. Han, D.J. Srolovitz, G. Ackland, D.Y. Sun, M. Asta, Philos. Mag. 83 (2003) 3977.
[19] W.D. Wilson, R.D. Johnson, in: P.C. Gehlen, J.R. BeelerJr., R.I. Jaffee (Eds.), Interatomic Potentials and Simulation of Lattice Defects, Plenum, 1972, p. 375.
[20] M.W. Finnis, J.E. Sinclair, Philos. Mag. A 50 (1984) 45, 'Erratum', Philos. Mag. A 53 (1986) 161.
[21] D.E. Beck, Mol. Phys. 14 (1968) 311.
[22] G. Kresse, J. Hafner, Phys. Rev. B 47 (1993) 558.
[23] G. Kresse, J. Hafner, Phys. Rev. B 49 (1994) 14251.
[24] G. Kresse, J. Furthmüller, Comput. Mater. Sci. 6 (1996) 15.
[25] G. Kresse, D. Joubert, Phys. Rev. B 59 (1999) 1758.
[26] P.E. Blöchl, Phys. Rev. B 50 (1994) 17953.
[27] C. Domain, A. Legris, Philos. Mag. 85 (2005) 569.
[28] K. Morishita, R. Sugano, B.D. Wirth, J. Nucl. Mater. 323 (2003) 243.
[29] C. Domain, C.S. Becquart, J. Foct, Phys. Rev. B 69 (2004) 144112.
[30] B. Bech Nielsen, A. van Veen, J. Phys. F: Met. Phys. 15 (1985) 2409.
[31] K. Morishita, B.D. Wirth, T. Diaz de la Rubia, A. Kimura, in: S. Hanada, Z. Zhong, S.W. Nam, R.N. Wright (Eds.), Proceedings of the The Fourth Pacific Rim International Conference on Advanced Materials and Processing (PRICM4), The Japan Institute of Metals, 2001, p. 1383.
[32] A.D. Le Claire, J. Nucl. Mater. 69&70 (1978) 70.
[33] B.D. Wirth, G.R. Odette, J. Marian, L. Ventelon, J.A. Young-Vandersall, L.A. Zepeda-Ruiz, J. Nucl. Mater. 329–333 (2004) 103.
[34] T. Seletskaia, Y. Osetsky, R.E. Stoller, G.M. Stocks, Phys. Rev. Lett. 94 (2005) 046403.
[35] C.C. Fu, F. Willaime, Phys. Rev. B 72 (2005) 064117.
[36] R.J. Kurtz, H.L. Heinisch, J. Nucl. Mater. 329–333 (2004) 1199.